Geophysical Journal International

Geophys. J. Int. (2013) **193,** 136–148 doi: 10.1093/gji/ggs122

Spectral and spatial decomposition of lithospheric magnetic field models using spherical Slepian functions

Ciarán D. Beggan,[1] Jarno Saarimäki,[2,*] Kathryn A. Whaler[2] and Frederik J. Simons[3]

[1] *British Geological Survey, Murchison House, West Mains Road, Edinburgh* EH9 3LA, *UK. E-mail: ciar@bgs.ac.uk*
[2] *School of GeoSciences, University of Edinburgh, West Mains Road, Edinburgh* EH9 3JW, *UK*
[3] *Department of Geosciences, Princeton University, Guyot Hall, Princeton,* NJ 08544, *USA*

Accepted 2012 December 21. Received 2012 December 9; in original form 2011 December 23

SUMMARY

Global magnetic field models are typically expressed as spherical-harmonic expansion coefficients. Slepian functions are linear combinations of spherical harmonics that produce new basis functions, which vanish approximately outside chosen geographical boundaries but also remain orthogonal within the spatial region of interest. Hence, they are suitable for decomposing spherical-harmonic models into portions that have significant magnetic field strength only in selected areas. Slepian functions are spatio-spectrally concentrated, balancing spatial bias and spectral leakage. Here, we employ them as a basis to decompose the global lithospheric magnetic field model MF7 up to degree and order 72, into two distinct regions. One of the resultant fields is concentrated within the ensemble of continental domains, and the other is localized over its complement, the oceans. Our procedure neatly divides the spectral power at each harmonic degree into two parts. The field over the continents dominates the overall crustal magnetic field, and each region has a distinct power-spectral signature. The oceanic power spectrum is approximately flat, while that of the continental region shows increasing power as the spherical-harmonic degree increases. We provide a further breakdown of the field into smaller, non-overlapping continental and oceanic regions, and speculate on the source of the variability in their spectral signatures.

Key words: Magnetic anomalies: modelling and interpretation; Satellite magnetics.

1 INTRODUCTION

The magnetic field of the Earth is one of the few measurable quantities that provide remote access to the internal dynamics of our planet (see, e.g. Thébault *et al.* 2010). For instance, past movements of tectonic plates may be inferred from the orientation of magnetic minerals in the crust, while the secular variation of the field at the surface gives insight into the properties of the outer core (Hulot *et al.* 2010).

This paper studies the global lithospheric magnetic field at the Earth's surface, focusing on the different signatures of the field over continents and oceans. On short timescales, the crustal field can be regarded as effectively constant in time, though its induced part does vary slightly (Thébault *et al.* 2009, 2010). The magnitude of the crustal field can vary from a fraction of a nanoTesla (nT) to thousands of nT at the Earth's surface. The continents comprise a number of ancient blocks with varying magnetic properties, while the oceanic crust is relatively young, thinner and appears much more homogeneous (Arkani-Hamed & Dyment 1996). It is generally assumed that at a global scale the continental regions mainly exhibit induced magnetization while the oceanic regions can contain both remanent and induced magnetization (Cohen & Achache, 1994; Dyment & Arkani-Hamed 1998). One manifestation of the remanent magnetization of the ocean floor is the 'striping' parallel to mid-ocean ridges, which is due to past reversals of the magnetic poles. The width of the stripes, from a few kilometres to tens of kilometres, reflects the combination of plate spreading rate and reversal frequency (Kono 2007).

Since the times of Gauss, planetary magnetic fields have been represented by the expansion of the potential in the basis of spherical harmonics (e.g. Backus *et al.* 1996; Langel & Hinze, 1998). From the 'spectral' representation in terms of spherical-harmonic 'Gauss' coefficients at individual degrees and orders, regional 'spatial' properties are difficult to deduce. The spherical harmonics are perfectly localized spectrally (Freeden & Michel 1999) but their spatial energy is geographically distributed over the entire globe. Information about the field contained in a single spherical-harmonic coefficient thus ultimately derives from a signal that may originate anywhere on the surface of the planet. Only by expanding the entire set of spherical harmonics back into the space domain do we regain a sense of the geographic distribution of the field—at the

[*] Now at: Astrock Geophysics, Finland.

expense of confounding its spectral properties. The situation is even worse when the spherical-harmonic coefficients are squared (which removes phase information) and summed over all orders, to report a (by this construction necessarily) isotropic 'power spectrum' or 'degree variance', at each individual degree. Here too, while we get an idea of the mean-squared value of the field at a certain spherical-harmonic degree, we remain ignorant of the distribution of precisely where, geographically, the field is prominently contributing to the power at that degree. In other words, spherical harmonics form a well-understood and convenient apparatus for the representation and analysis of magnetic fields globally, but they lack the flexibility to identify the spatial and spectral structure of such fields from a 'spatio-spectrally' mixed vantage point.

One of the early attempts at bringing spatial selectivity to spherical-harmonic-based representations involved an approach reminiscent of 'wavelet' analysis (Simons *et al.* 1997). Spatially selective windows targeting a particular spectral degree range were designed, and a space-spectral analysis conducted via a convolutional approach. The drawback of wavelets and their relatives is that the area of the spatial region over which information is being extracted scales inversely with the spherical-harmonic degree range of interest. Large-degree (high spatial frequency) information derives from small areas, small-degree (low spatial frequency) structure is obtained from larger regions.

To study the spectral behaviour of a geophysical signal confined to a particular geographic region of interest, a different solution must be sought. Suppose we were to window the data over a spatial region of interest using a simple multiplicative binary mask (e.g. Peebles 1973; Wandelt *et al.* 2001; Dahlen & Simons, 2008). In the spectral domain, this operation would essentially correspond to a convolution of the spherical-harmonic expansion coefficients of the data with those of the mask itself. A binary mask, while perfectly localized in the space domain, has an infinite dimensional ringing behaviour in the spectral domain. The analysis operation would thus lead to results displaying undesirable spectral-domain artefacts. Evidently some way of 'tapering' the 'boxcar' must be found, by which some spatial selectivity is sacrificed in return for spectral windows that have better sidelobe behaviour (Tegmark 1996, 1997). Such procedures, known as 'apodization', were first cast as an optimization problem for application to time-series analysis in the 1960s (see, e.g. Slepian 1983).

With spherical Slepian functions (Wieczorek & Simons 2005; Simons *et al.* 2006) the trade-off between spectral and spatial concentration on the surface of the unit sphere is optimized, by constructing a particular linear combination of spherical harmonics. This combination is such that while bandlimited within a certain spectral interval of interest, the functions maximize their spatial energy over a certain spatial region of interest, preserving orthogonality over the entire sphere as well as over the chosen spatial domain. The trade-off arises because bandlimited expansions cannot be spatially limited, or vice versa, which is a consequence of the Paley–Wiener theorem (Daubechies 1992; Mallat 1998), and because spatial concentration is inversely proportional to spectral concentration, which is a consequence of the Heisenberg inequality (Percival & Walden 1993; Narcowich & Ward 1996; Freeden & Michel 1999; Wieczorek & Simons 2005).

Only one Slepian function is the spatially 'best'-concentrated function for a given target region R on the surface of the sphere Ω. The complete solution to the 'concentration problem' as put forth by Simons *et al.* (2006) contains an entire basis set of functions which are eigenfunctions of the spatio-spectral localization (bandlimitation followed by spatial limitation) projection operator. These eigenfunctions are all orthogonal to each other over the region R, which can have an arbitrarily complex shape, and they are furthermore also orthogonal over the entire globe Ω. The eigenvalues embody the level to which the energy of the spatial functions is confined to the region of interest R. Well-concentrated functions are 'large' within the region and have eigenvalues close to one. These can be used to approximate bandlimited signals inside the region of interest. The rest of the set consists of poorly concentrated, nearly-zero-eigenvalue functions that are 'small' within R but large in the complementary region $\Omega\backslash R$. Those functions are suitable for approximating bandlimited signals outside the spatial region of primary interest.

Taken together, the Slepian basis set is merely a unitary linear transformation of the spherical-harmonic basis, but it is the spatial region of interest, built into their construction via quadratic maximization, that leads to their efficiency for modelling regional signals. A small subset is 'large' in the region R, the vast majority is 'small' over R. The double orthogonality of the Slepian functions, both over R and over $\Omega\backslash R$ is a property that is convenient and very welcome on statistical grounds, for example, when inversions for the source or estimations of the power spectral density of the field components or the overall potential are being made on the basis of actual satellite data (Simons & Dahlen 2006; Dahlen & Simons 2008; Simons *et al.* 2009; Plattner & Simons 2013). No such attempts are being made here. It finally should be stated that other data-based inversion approaches may provide the desired (double) orthogonality of the basis functions (e.g. Hwang 1993; Górski 1994; Xu 1998; Schachtschneider *et al.* 2010, 2012; Slobbe *et al.* 2012), but Slepian functions are the only ones that achieve this feat in a fully analytical, and easily computable framework, from prior considerations of the geometry of the region of interest or data availability.

In summary, and relating back to the objective in this paper, which is to study the spectral signature of the Earth's magnetic field over continents and oceans separately, the Slepian functions provide an optimal basis, or else, a set of windowing functions, to model, analyse or represent, the magnetic potential within non-overlapping geographical regions. In a decomposition where the entire bandwidth of the original model is being used, but selectively truncated expansions into Slepian functions are formed from the original spherical-harmonic coefficients, the fit of the signal within individual geographical regions is effectively maximized, while at the same time, edge effects, which lead to distortions in their spherical-harmonic representations, are minimized. Counil *et al.* (1991) demonstrated that differences between the field in continental and oceanic crust modelled exclusively using spherical-harmonic functions may be influenced by edge effects. Using Slepian functions, global signals can be decomposed into effectively regional models that best approximate and thus separate the field over the areas of interest, and whose spherical-harmonic spectrum can be studied robustly. Ultimately, our objective should be to use the separation of the magnetic fields over the continents and oceans for geological inference of the magnetization structure of the respective domains (e.g. Gubbins *et al.* 2011), but this goal remains out of the scope of the present contribution.

The Slepian decomposition method can be applied to magnetic fields from other planetary bodies with sufficient spherical-harmonic model resolution and identifiable regions of interest. The technique can also be used in other areas where spatial data are commonly described by spherical harmonics such as ocean or glacial signals in gravity models (e.g. Reigber *et al.* 2005; Slobbe *et al.* 2012; Harig & Simons 2012) or when interpreting seismic shear

wave velocity models (e.g Becker & Boschi 2002; Ritsema *et al.* 2010) but also in astrophysics (e.g. Peebles 1973; Hauser & Peebles 1973) and cosmology (e.g. Tegmark 1997; Oh *et al.* 1999).

Regional modelling can be achieved by other methods, such as via harmonic splines (Shure *et al.* 1982 1985; Amirbekyan *et al.* 2008), (Revised) Spherical Harmonic Cap Analysis (Haines 1985; Thébault *et al.* 2006) and various other localizing techniques including wavelets (e.g. Holschneider *et al.* 2003; Lesur 2006). Each method has advantages over global spherical-harmonic analysis for local regions. Schott & Thébault (2011) discuss the merits and limitations of each approach in detail. However, none of the above techniques attempts to formally optimize field separation over arbitrary regions with irregular boundaries from a global model consisting of spherical-harmonic coefficients. In this respect the approach by Slepian functions is unique and suited to the problem of studying the contributions to the global spherical-harmonic power spectrum that arise from distinct geographic regions, continents and oceans, and to assess their spectral characteristics individually.

Several high-quality lithospheric field models are available for study. Much use has been made of the excellent satellite vector data available from the Ørsted, CHAMP and SAC-C missions between 1999 and 2010. Models of the lithospheric field include satellite data-only models such as MEME (Thomson *et al.* 2010) and POMME7 (Maus *et al.* 2010), and models including data from surface, marine and aeromagnetic surveys such as EMAG2 (Maus *et al.* 2009). The spherical-harmonic expansion coefficients of these lithospheric models (the 'Gauss coefficients') typically agree to about degree 80. We restrict our study to the crustal field between spherical-harmonic degrees 16–72 using the Gauss coefficients from the MF7 model (Maus *et al.* 2007). Further improvements to lithospheric field models are anticipated with data from the ESA Swarm satellite mission (Friis-Christensen *et al.* 2006).

We use a spherical Slepian-function decomposition of the field over the continents and their complement, the oceans, to investigate the differences between the field over those regions that can be identified from the spherical-harmonic power spectra. In Section 2 we review some basics of the spherical Slepian-function decomposition and establish the framework for its description. Originally developed as low-pass bandlimited functions, we also describe a decomposition using bandpass Slepian functions. For both of these we demonstrate how to decompose a field model of Gauss coefficients into separate regions. In Section 3 we present the results for the crustal magnetic field with an analysis of the trade-off between spatial and spectral accuracy that arises from the spectral coupling between each region. In Section 4 we discuss our findings and Section 5 concludes the paper.

2 METHODOLOGY

Before we proceed, we should caution the reader that history has decided that the commonly used symbol for the scalar Gauss expansion coefficients of the potential at spherical-harmonic degree l and order m should be g_l^m. In more recent history (e.g. Simons *et al.* 2006; Simons & Dahlen 2006), we have used $g_\alpha(\theta, \phi)$ for the αth bandlimited scalar Slepian function evaluated at colatitude θ and longitude ϕ on the unit sphere, and $g_{\alpha,lm}$ for the expansion coefficients of the Slepian functions in the spherical-harmonic basis. When we collect the coefficients $g_{\alpha,lm}$ for the αth Slepian functions into a (column) vector, we write $\mathbf{g}_\alpha$, when we collect the expansion coefficients of all of the Slepian functions, column by column, in to a matrix, we write the results as $\mathbf{G}$, and when we collect the Slepian functions themselves, evaluated as a function of colatitude and longitude, into a column vector, we write $\mathbf{g}(\theta, \phi)$. At the risk of antagonizing our forebears we shall use v_l^m for the (Gauss) expansion coefficients of the potential V, and collect them in a column vector $\mathbf{v}$.

2.1 Spherical harmonics

Magnetic fields originating inside or outside the Earth can be approximated by a scalar potential V that satisfies Laplace's equation,

$$\nabla^2 V = 0, \tag{1}$$

that is, it is harmonic outside the source region. From this potential, the magnetic field $\mathbf{B}$ is obtained by

$$\mathbf{B} = -\nabla V. \tag{2}$$

In spherical coordinates (r, θ, ϕ) the harmonic potential of the internal field is conveniently represented by a spherical-harmonic expansion to a certain bandwidth L,

$$V(r, \theta, \phi) = a \sum_{l=1}^{L} \left(\frac{a}{r}\right)^{l+1} \sum_{m=-l}^{l} v_l^m Y_l^m(\theta, \phi), \tag{3}$$

where $Y_l^m(\theta, \phi)$ is a real spherical surface harmonic of degree l and order m, the Gauss coefficients v_l^m define the weightings of the individual harmonics, and a is a reference radius for the expansion (typically the Earth's mean radius, 6371.2 km), which is valid when $r \geq a$. Here, the v_l^m and v_l^{-m} replace the g_l^m and h_l^m in the traditional geomagnetic notations.

Spherical surface harmonics are orthogonal over the whole sphere Ω: when $l \neq l'$ or $m \neq m'$,

$$\int_\Omega Y_l^m(\theta, \phi) Y_{l'}^{m'}(\theta, \phi)\, \mathrm{d}\Omega = 0. \tag{4}$$

In geomagnetism, the normalization (i.e. the non-zero value of eq. 4 when $l = l'$ and $m = m'$) is usually that due to Schmidt (see Blakely 1996). The spherical-harmonic power spectrum R_l is then defined as the squared magnitude of the magnetic field at degree l averaged over a spherical surface of radius r, which, in this Schmidt normalization, amounts to (Mauersberger 1956; Lowes 1966, 1974; Sabaka *et al.* 2010):

$$R_l(r) = (l+1)\left(\frac{a}{r}\right)^{2l+4} \sum_{m=-l}^{l} \left(v_l^m\right)^2. \tag{5}$$

We do not speak of 'spectral densities' since we do not report averages per spherical-harmonic degree but rather totals. A 'flat' power spectrum in the sense of eq. (5) is not 'white', as 'whiteness' should imply that the spatial autocorrelation is a delta function (Dahlen & Simons 2008, their eqs 33 and 34). It is important to heed the implications of this particular definition for a physical interpretation (Hipkin 2001; Maus 2008).

2.2 Slepian functions

2.2.1 Notation and objective

Spherical surface harmonics are functions of global support that can be converted, by a unitary linear transformation, into a spherical Slepian basis whose energy is concentrated onto specific patches of the sphere (Wieczorek & Simons 2005; Simons *et al.* 2006). A detailed review of the construction and properties of 1-, 2- and 3-D

Slepian functions is given by Simons (2010). Here, we present a slightly different notation from that previously used by these authors. Both notations are equivalent, but in this paper we rely more on vector–matrix operations than on the explicit summations that have been mostly used elsewhere. First, we consider some elementary mathematical definitions.

To allow for computations other than in geomagnetism, we include the $l = 0$ monopole term in what follows. Spherical surface harmonics up to degree and order L can be expressed as a vector of $(L + 1)^2$ elements, each of which is a function of position (θ, ϕ) on the unit sphere:

$$\mathbf{y}(\theta, \phi) = \left[Y_0^0(\theta, \phi) \cdots Y_l^m(\theta, \phi) \cdots Y_L^L(\theta, \phi) \right]^{\mathrm{T}}. \tag{6}$$

The ordering of the spherical harmonics Y_l^m is naturally arbitrary. The notation is such that all boldface lower-case characters represent column vectors and boldface upper-case represents matrices. In geomagnetism, the monopole harmonic (Y_0^0) is usually ignored (or set to zero), but we include it in this analysis to prevent loss of generality for other applications.

On a unit sphere, the potential $V(\theta, \phi)$ up to degree L is represented in a spherical-harmonic basis by a single $(L + 1)^2$-dimensional column vector of Gauss coefficients, $\mathbf{v}$. The potential on the surface is obtained from these Gauss coefficients as

$$V(\theta, \phi) = \mathbf{v}^{\mathrm{T}}\mathbf{y}(\theta, \phi) = \mathbf{v} \cdot \mathbf{y}(\theta, \phi). \tag{7}$$

The representation of the potential in a spherical-harmonic spectral-domain basis by the lower-case boldface symbol $\mathbf{v}$, which lacks a dependence on (θ, ϕ) distinguishes it from the space-domain potential $V(\theta, \phi)$ in our notation.

Spherical Slepian functions (hereafter simply: Slepian functions) are an alternative basis,

$$\mathbf{g}(\theta, \phi) = \left[g_1(\theta, \phi) \cdots g_\alpha(\theta, \phi) \cdots g_{(L+1)^2}(\theta, \phi) \right]^{\mathrm{T}}. \tag{8}$$

Each of the entries in eq. (8) is a basis function that is linearly related to the surface harmonics by the expansion

$$g_\alpha(\theta, \phi) = \mathbf{g}_\alpha^{\mathrm{T}}\mathbf{y}(\theta, \phi) = \mathbf{g}_\alpha \cdot \mathbf{y}(\theta, \phi). \tag{9}$$

As in eq. (7), our notation distinguishes the spatial-domain Slepian functions $g_\alpha(\theta, \phi)$ from their expansion coefficients $\mathbf{g}_\alpha$ in the spherical-harmonic basis. Slepian basis functions are orthonormal over the unit sphere so that

$$\mathbf{g}_\alpha \cdot \mathbf{g}_{\alpha'} = \begin{cases} 1 & \text{if } \alpha = \alpha', \\ 0 & \text{otherwise.} \end{cases} \tag{10}$$

The Slepian basis $\mathbf{g}(\theta, \phi)$ is produced from the spherical surface harmonic basis $\mathbf{y}(\theta, \phi)$ by multiplying the latter by the unitary matrix which is given by

$$\mathbf{G}^{\mathrm{T}} = \begin{bmatrix} \mathbf{g}_1^{\mathrm{T}} \\ \vdots \\ \mathbf{g}_{(L+1)^2}^{\mathrm{T}} \end{bmatrix}, \qquad \mathbf{G}\mathbf{G}^{\mathrm{T}} = \mathbf{I}. \tag{11}$$

The matrix $\mathbf{G}$ is constructed by optimization, as will be shown in the next section, to localize the solution over specified areas or regions (and their complements), for a given bandwidth L. Note that the regions of interest do not have to be connected or contiguous, but they must be non-overlapping to preserve orthogonality between different constructions. For the case of unconnected continental regions on the Earth, and the complementary oceanic domain, a single optimization procedure determines a complete set of basis functions, which naturally separates into those basis functions that are well localized over either of the two distinct domains:

$$\mathbf{G}^{\mathrm{T}}\mathbf{y}(\theta, \phi) = \begin{bmatrix} \mathbf{G}_{\mathrm{in}}^{\mathrm{T}}\mathbf{y}(\theta, \phi) \\ \mathbf{G}_{\mathrm{out}}^{\mathrm{T}}\mathbf{y}(\theta, \phi) \end{bmatrix} = \begin{bmatrix} g_1(\theta, \phi) \\ \vdots \\ g_K(\theta, \phi) \\ g_{K+1}(\theta, \phi) \\ \vdots \\ g_{(L+1)^2}(\theta, \phi) \end{bmatrix} = \begin{bmatrix} \mathbf{g}_{\mathrm{in}}(\theta, \phi) \\ \mathbf{g}_{\mathrm{out}}(\theta, \phi) \end{bmatrix}, \tag{12}$$

where the index K denotes the last element of the functions primarily concentrated in the first domain, subscripted 'in' (that is, inside the region of interest), and $K + 1$ denotes the first element of the functions concentrated in the other domain, subscripted 'out' (outside the region of interest, inside of the complement). The basis functions of domain 'in' are approximately non-zero only within the chosen region R, while those of domain 'out' are concentrated outside R. The value of K depends on the bandwidth and the fractional area of the 'in' region. With this type of a spherical harmonic-to-Slepian transformation we restrict ourselves to analysing only one spherical shell (e.g. the surface) at a time. Simons & Dahlen (2006, their section 6.3) discuss aspects of harmonic continuation using the Slepian basis.

2.2.2 *Determination of the Slepian basis*

The Slepian functions span a linear subspace of $\mathbf{y}(\theta, \phi)$ in which the energy, or sum-squared function value, over R is maximized. At this point the geometry of the region under consideration enters the calculation. We compute the Gram matrix of energy in R as

$$\mathbf{D} = \int_R \mathbf{y}(\theta, \phi)\mathbf{y}^{\mathrm{T}}(\theta, \phi)\, \mathrm{d}\Omega \tag{13}$$

$$= \int_R \begin{bmatrix} Y_0^0 Y_0^0 & \cdots & Y_0^0 Y_L^L \\ \vdots & \ddots & \vdots \\ Y_0^0 Y_L^L & \cdots & Y_L^L Y_L^L \end{bmatrix} \mathrm{d}\Omega. \tag{14}$$

This 'localization' matrix is symmetric and the subspace of maximum energy is readily obtained by eigenvalue decomposition. The eigenvalues and eigenvectors of $\mathbf{D}$ are defined as

$$\mathbf{D}\mathbf{G} = \mathbf{G}\mathbf{\Lambda}, \tag{15}$$

where each column of $\mathbf{G}$ contains one eigenvector and $\mathbf{\Lambda}$ is a diagonal matrix with the corresponding eigenvalues,

$$\mathbf{\Lambda} = \mathrm{diag}\left(\lambda_1, \cdots, \lambda_\alpha, \cdots, \lambda_{(L+1)^2}\right). \tag{16}$$

The symmetry of $\mathbf{D}$ provides that all eigenvalues are real and positive (or zero) and that all eigenvectors are orthogonal, which makes $\mathbf{G}$ unitary. Furthermore, each eigenvalue λ_α defines the fractional energy (over R compared to Ω) that is represented in the projection $g_\alpha(\theta, \phi) = \mathbf{g}_\alpha \cdot \mathbf{y}(\theta, \phi)$. The eigenvalue problem (15) is equivalent to the maximization of λ for functions given the available bandwidth L. The Slepian functions in this discussion have been perfectly bandlimited spectrally, to degree and order L.

The eigenvalues λ_α are characterized by a spectrum of near-unity values separated from near-zero values by a narrow transition region. This shape is the motivation for the heuristic decomposition into K 'in' and $(L+1)^2 - K$ 'out' functions, where $\lambda_K \approx 0.5$. It is generally not possible to separate perfectly the energy of the functions that concentrate inside and outside R in this manner. Hence, there will be spatial leakage between the two domains 'in' and 'out', and the energy of the leakage depends on the eigenvalues, which are close to (but smaller than) one, $\lambda_\alpha \lesssim 1$, when $\alpha \leq K$, and greater than (but close to) zero, $\lambda_\alpha \gtrsim 0$, when $\alpha > K$.

The diagonalization is reminiscent of Principal-Component Analysis (PCA, e.g. Jolliffe 2002) with the exception that PCA traditionally finds linear subspaces that concentrate data variance rather than basis-function energy. Slepian eigenvectors and eigenvalues can also be considered to result from singular-value decomposition (SVD) if we consider the integral in (14) as a 'normal' matrix, the product of a matrix and its transpose, as arises in inversion problems (Simons 2010). The elements of $\mathbf{D}$ are evaluated by numerical integration, or analytically in certain circumstances; see Wieczorek & Simons (2005) and Simons *et al.* (2006, 2009). When the region of concentration has the symmetry of a polar cap or an antipodal pair of polar caps (Simons & Dahlen 2006), the matrix $\mathbf{G}$ can be found without the intermediary of $\mathbf{D}$, through commutation relations. Numerically, this property is very attractive.

The eigenvalues λ_α cannot exceed unity because no orthonormal projection can provide more fractional energy than any of the spherical surface harmonics over the whole sphere. For eigenvalues near one, most of the energy of the projection is contained within R. When the eigenvalues are near zero, most energy of the projection is contained outside R. The sum of the eigenvalues λ_α gives the 'Shannon number' (Simons *et al.* 2006), which can directly be computed from

$$K = (L+1)^2 \frac{A}{4\pi}, \tag{17}$$

where A is the surface area (in steradians) of R. The Shannon number, a space–bandwidth product, approximates the dimension of the space of approximately space- (to R) and band- (to L) limited functions on the sphere. It corresponds to the number of functions that usefully project the energy of the spherical harmonics onto the target region R.

It is reasonable to omit certain spherical-harmonic degrees from the Slepian functions if there is no energy in those degrees. For instance, in crustal field models, due to the inability to separate the dominant core field contribution at degrees $l = 12$–15, Gauss coefficients of degrees $l < l_0 = 15$ are generally set to zero. In such a case, the corresponding Slepian basis (8) has $(L+1)^2 - l_0^2$ elements and the Shannon number, modified after (17), would be

$$K = \left[(L+1)^2 - l_0^2\right] \frac{A}{4\pi}. \tag{18}$$

There are corresponding changes in all related equations that refer explicitly to the dimensions of vectors and matrices, which are, however, straightforward to adapt. The resulting models would thus be based on bandpass Slepian functions rather than the low-pass ones which have been the subject of all previous work using spherical Slepian functions known to us.

2.2.3 Decomposition of the Gauss coefficients

A harmonic potential $V(\theta, \phi)$ can thus be decomposed into parts (almost) localized inside and outside a region R as follows:

$$V_{\text{in}}(\theta, \phi) = \left(\mathbf{G}_{\text{in}}^{\text{T}}\mathbf{v}\right)^{\text{T}} \mathbf{g}_{\text{in}}(\theta, \phi), \tag{19}$$

$$V_{\text{out}}(\theta, \phi) = \left(\mathbf{G}_{\text{out}}^{\text{T}}\mathbf{v}\right)^{\text{T}} \mathbf{g}_{\text{out}}(\theta, \phi). \tag{20}$$

The potential over the entire sphere is a superposition of these partial expansions,

$$V(\theta, \phi) = V_{\text{in}}(\theta, \phi) + V_{\text{out}}(\theta, \phi). \tag{21}$$

Furthermore, the spherical-harmonic representations of the two regional potentials become the projections

$$\mathbf{v}_{\text{in}} = \left(\mathbf{G}_{\text{in}}\mathbf{G}_{\text{in}}^{\text{T}}\right)\mathbf{v}, \tag{22}$$

$$\mathbf{v}_{\text{out}} = \left(\mathbf{G}_{\text{out}}\mathbf{G}_{\text{out}}^{\text{T}}\right)\mathbf{v}. \tag{23}$$

Eqs (22) and (23) imply a transfer of energy from each of the spherical-harmonic elements in the original to the individual regional expansions, although the matrices $(\mathbf{G}_{\text{in}}\mathbf{G}_{\text{in}}^{\text{T}})$ and $(\mathbf{G}_{\text{out}}\mathbf{G}_{\text{out}}^{\text{T}})$ are diagonally dominant. There is a trade-off between the spectral coupling and the spatial leakage from one domain to another: decreasing the amount of coupling will tend to increase the spatial bias by reducing the regional selectivity of the decomposition. The behaviour can be understood on the basis of the detailed considerations made by Simons & Dahlen (2006) for the case where linear functionals of the data result in signal estimation from noisy and incomplete observations, and by Dahlen & Simons (2008) who treated the case where quadratic data functionals result in direct estimates of the power-spectral density from similar observations. There are more connections implicit in the early theoretical work by Kaula (1967), Spencer & Gubbins (1980), Whaler & Gubbins (1981), and in the practical studies by Slobbe *et al.* (2012), Trampert & Snieder (1996) and Schachtschneider *et al.* (2010), to name a few examples from geodesy, seismology and geomagnetism, respectively. However, the material in this section does not appear explicitly in those papers, nor has the algorithm proposed in the next section been applied before.

2.2.4 Algorithm

We have implemented the ocean–continent magnetic-field decomposition using the following five algorithmic steps for which we have made the computer code freely available:

(i) A file containing the latitudes and longitudes of the boundary outlines was generated to determine the spatial region of interest R. The average spacing between points was approximately 10 km.

(ii) A localization matrix $\mathbf{D}$ was computed for the region of interest on the sphere using eq. (14) with the bandwidth $L = 72$. This is the most time-consuming step, which, however, benefited from a parallel implementation which reduced computation time to a matter of minutes on a contemporary eight-processor machine.

(iii) Slepian basis functions for the region were generated using the eigenvector decomposition of the localization matrix of eq. (15). They were sorted by eigenvalue, from the largest to the smallest.

(iv) The spherical-harmonic coefficients were converted into equivalent Slepian coefficients using eqs (19) and (20).

(v) The Shannon number K was used to separate the Slepian coefficients into the two complementary regions of interest, and the Slepian coefficients were transformed back to spherical-harmonic coefficients using eqs (22) and (23).

The spherical-harmonic coefficients for each region can be treated as usual, for example, to find field components at a series of points for plotting in map form, or squared, summed and scaled to give a power spectrum as per eq. (5). With regards to this last operation, it is to be noted that this does not amount to a 'multitaper' power spectral estimate in the sense of Wieczorek & Simons (2007) or Dahlen & Simons (2008, their eqs 130 and 139). In the present approach we focused on containing spatial bias by achieving field separability over both regions at the full resolution of the data. As shown in the previous section and in the examples to follow, this leads to a spectral coupling with a manageable bias, or effective bandwidth of resolution, for the spectral estimate, whose variance, unlike in both studies cited, we did not attempt to minimize. The advantage of our present approach is that it stays intuitively close to geomagnetic practice while alleviating the drawbacks of forming 'periodogram' spectral estimates with simple binary masks for the continents and the oceans—a case treated in detail by Dahlen & Simons (2008, their section 5). Field separation and spectral estimation are different statistical problems, one linear in the data and the other quadratic: our approach of basis projection, truncation and reprojection, for evaluation in the space domain and spectral estimation, serves a dual purpose that is closer in spirit to the former, without excessively violating the basic premise of the latter. Lewis & Simons (2012) can be consulted for an example for the Martian lithospheric field, where the focus lies on the estimation and parameterized inversion of the power spectrum rather than on separable field representation with the quadratic spectrum as a by-product, as is our case.

3 CRUSTAL FIELD DECOMPOSITION

The lithospheric field decomposed is the model MF7 of Maus *et al.* (2007), which extends to spherical harmonic degree 133. This model, derived for use at the Earth's mean radius (6371.2 km), is based on CHAMP satellite measurements up to April 2010. The model is suitable for the analysis of long-wavelength features of the lithospheric field, as shorter wavelengths become distorted due to data processing and model regularization. We thus examine the field at the spherical-harmonic degrees $l = 16$–72, as degrees beyond 72 are subject to along-track filtering of the data and stronger *a priori* smoothing (Maus *et al.* 2008). The boundaries of the continental crust are approximated from global relief images of the NOAA ETOPO2v2 map. In most regions these images show clear features at the edges of continental and oceanic regions, which can be confirmed by comparison with oceanic crust boundaries of Müller *et al.* (2008) or Counil *et al.* (1991) among others.

Fig. 1 shows the radial component of the magnetic field of MF7 along with the continental boundaries. We employ Slepian functions to decompose the scalar potential into the continental domain and its complement, the oceanic domain. The figure includes the shoreline as a reference so that submarine continental crust is also distinguishable. We use the radial component of the magnetic field to assess the decompositions visually in the following sections. We analyse the results by studying spherical-harmonic power spectra (eq. 5), even though the optimal decomposition of the potential is not necessarily also optimal for its field components (Plattner *et al.* 2012). The number of Slepian eigenfunctions and their eigenvalues for each region is computed using the appropriate Shannon numbers from eqs (17) or (18). Some large-scale lithospheric anomalies are missing from the model, because the lowest spherical-harmonic degree considered is 16. Purucker *et al.* (2002) have argued that the large anomalies in southern North America could be the edge effects of large-scale cratonic magnetization, which is not contained in truncated lithospheric field models. In this paper we cannot study magnetization of the continents or the oceans, only the magnetic field itself and how it is expressed over the individual domains.

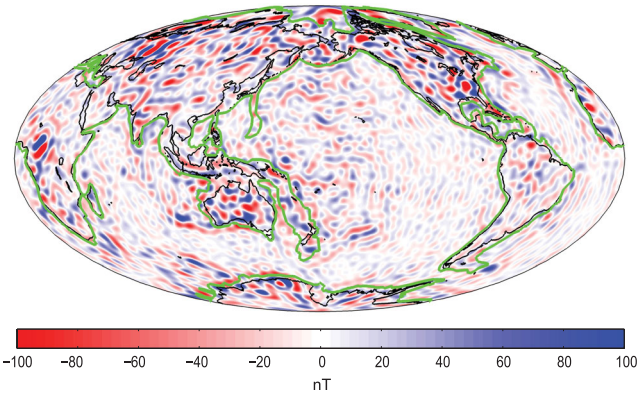

Figure 1. The radial component of the crustal magnetic field MF7 (Maus *et al.* 2007) for the spherical harmonic degrees $l = 16$–72 (units: nT). The green line shows the continental crust boundaries and the black line denotes the shorelines for reference. The colour scale is saturated: the field values reach a minimum of −288 nT and a maximum of 397 nT in places.

3.1 Decomposition using low-pass Slepian functions

From the MF7 model we use the first 5328 Gauss coefficients (up to degree and order 72) and include the g_0^0 coefficient (set to zero, as are degrees 1–15) for the purposes of the Slepian decomposition. A symmetric (5329 × 5329) localization matrix $\mathbf{D}$ of eq. (14) is computed from a list of 10 151 (latitude, longitude) pairs representing the continental shelf boundary, closed by spline interpolation. The eigenvectors of the localization matrix are sorted by decreasing eigenvalue and then the Gauss coefficients are converted into the equivalent complete description by Slepian function coefficients.

Fig. 2 shows the radial components of the continental and the oceanic signals expressed in the Slepian basis. In both cases, the signal outside the chosen area is very small, though in neither case does it vanish completely. Moreover, certain features generate systematic reverberation, or ringing, in the adjacent regions—such as that of continental signal south of Australia (upper panel). The computed Shannon number assigns 2170 Slepian basis functions to the continental crust and 3159 to the oceanic crust. Judging from the corresponding eigenvalues, about 5.0 per cent of the energy of the continental basis is outside of the boundaries; while for the oceanic basis, some 3.4 per cent leaks into the continental domain. From a spatial integration of the original signal and its comparison to the reconstruction over the partial domains, more than 98.2 per cent of the energy of the spatial signal is recovered in the continents, while 94.9 per cent is recovered over the oceans.

Fig. 3 shows the power spectra of the decomposed signals. In using eq. (5) for the computations in the case of the decomposed fields, we continue to refer to the surface area of the entire sphere, even though we have effectively zeroed out the contributions from the regions outside those of interest. A different definition of 'power' spectrum might have scaled our results by the areas of the region of interest. On the other hand, a different interpretation of our

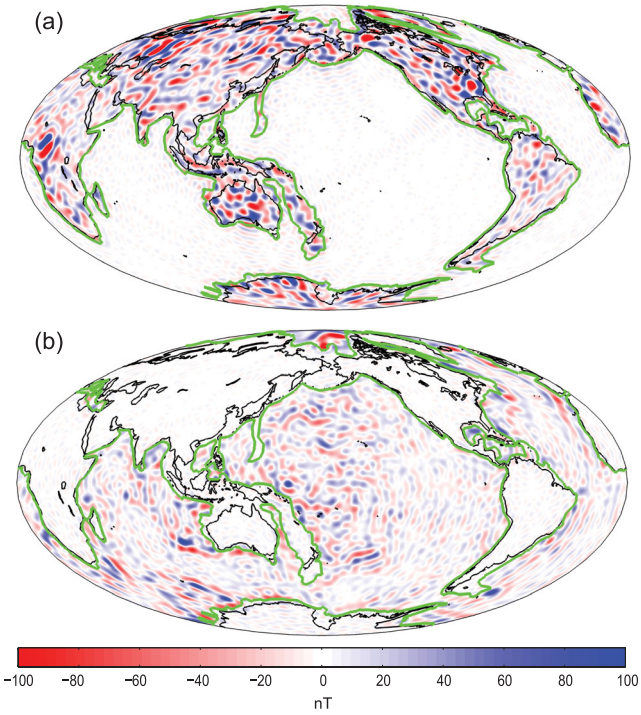

Figure 2. The radial component of the MF7 magnetic field data decomposed into (a) continental and (b) oceanic signals (units: nT). This decomposition uses low-pass Slepian functions that include spherical-harmonic degrees 0–72, although the input model contains only degrees 16–72. The separation of the basis set happens at the Shannon number, $K = 2170$ for the continents, which leaves 3159 functions to approximate the signal over the oceans.

computations might thus interpret our comparative results as 'energy' spectra rather than power spectra. Whatever the preference of the reader, the computer code that accompanies this paper can be easily adapted to make accommodations for taste.

For the oceanic region, degree 16 and the highest degrees (around 70) stand out. Degree 16 corresponds approximately to a wavelength of 2500 km, possibly present in the (north–south) direction parallel to the mid-ocean ridges. Degree 70 corresponds approximately to wavelengths of 550 km, which is perhaps the longitudinal wavelength of the north–south oriented magnetic 'stripes' visible to satellites in the Atlantic basin. The spectrum of the continental region shows much more variability than the oceanic signal. There are many peaks that follow those of the global spectrum. The peak at degree 25 is present in the oceanic signal but otherwise the large peaks are limited to the continents. Overall, the power from the continental region is significantly greater than the power of the oceanic region. This is most likely owing to the larger volume of magnetic rocks in the continents despite their smaller areal extent.

Fig. 3 also shows explicitly that the power spectrum of the sum of the decomposed signals is identical to the global spectrum of the original, while it can be shown that the sum of the partial spectra is a good, though not perfect, approximation to the global spectrum. We also see that there is some spectral leakage into the degrees below 16, though this is quite low compared to the power elsewhere. At this point, we also note that we have decomposed other lithospheric field models including MF6 (Maus *et al.* 2008) and POMME (Maus *et al.* 2010) which gave similar results to those shown in Figs 2 and 3.

3.2 Decomposition using bandpass Slepian functions

Fig. 4 shows the power spectra for the model decomposed in bandpass Slepian functions of degrees $l = 16$–72. The results are similar to the low-pass $l = 0$–72 decomposition shown in Fig. 3. Spatial leakage is slightly more prominent than previously, as deduced from the eigenvalues of the solution: 5.7 per cent of energy out of the continental basis and 3.6 per cent from the oceanic basis. For example, at the North Pole (plot not shown) the leakage of continental signal is more pronounced, though overall the spatial leakage is still quite small.

In the oceanic spectrum, the peak at degree 16 is stronger than for the low-pass Slepian functions, since with the bandpass functions, coupling to the degrees 0–15 is excluded. There are also power increases at higher degrees.

3.3 Individual continents and ocean basins

We next decompose the field model MF7 into five continental areas—Americas (North, Central and South), Africa, Eurasia, Australia and Antarctica—and four ocean basins—Atlantic, Pacific, Indian and North Pole. The field over each decomposed region is calculated from the original MF7 magnetic potential model (not from the decomposed components of the previous sections). Each time, the separation was performed using the appropriate Shannon number for the area under consideration.

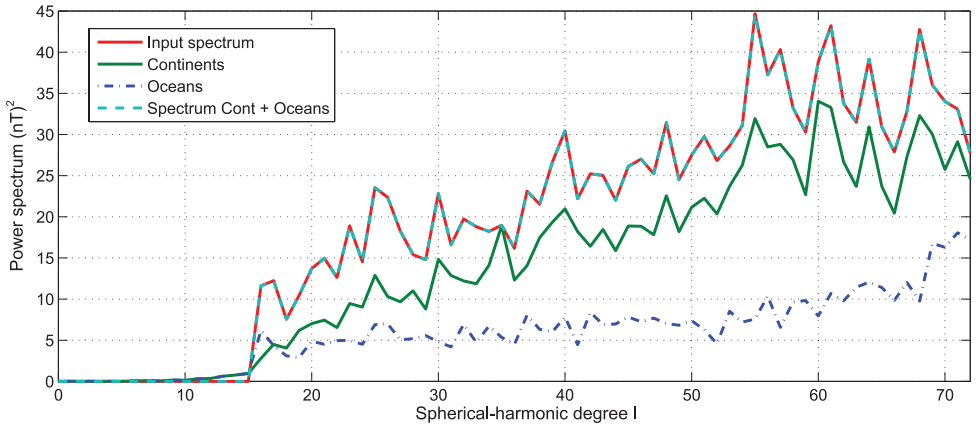

Figure 3. Power spectra of the crustal magnetic field MF7, globally ('input'), and with the signals decomposed into continental and oceanic domains using low-pass Slepian functions that contain all spherical-harmonic degrees from 0 to 72. Also shown is the spectrum of the sum of the continent and ocean model fields, which is identical to the global spectrum. Units: nT^2.

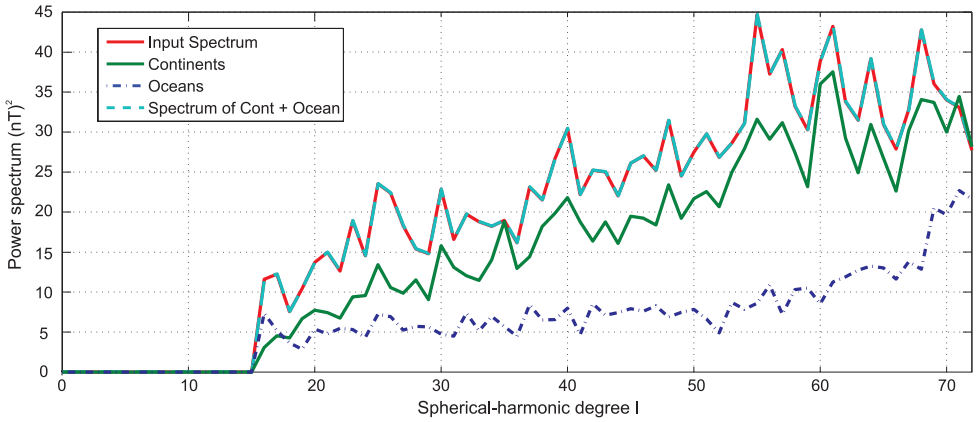

Figure 4. Power spectra of the crustal magnetic field MF7, globally, and with the signals decomposed using bandpass Slepian functions that contain only spherical-harmonic degrees between 16 and 72, and the spectrum of the sum of the decomposed model fields, as described in the text. Units: nT^2.

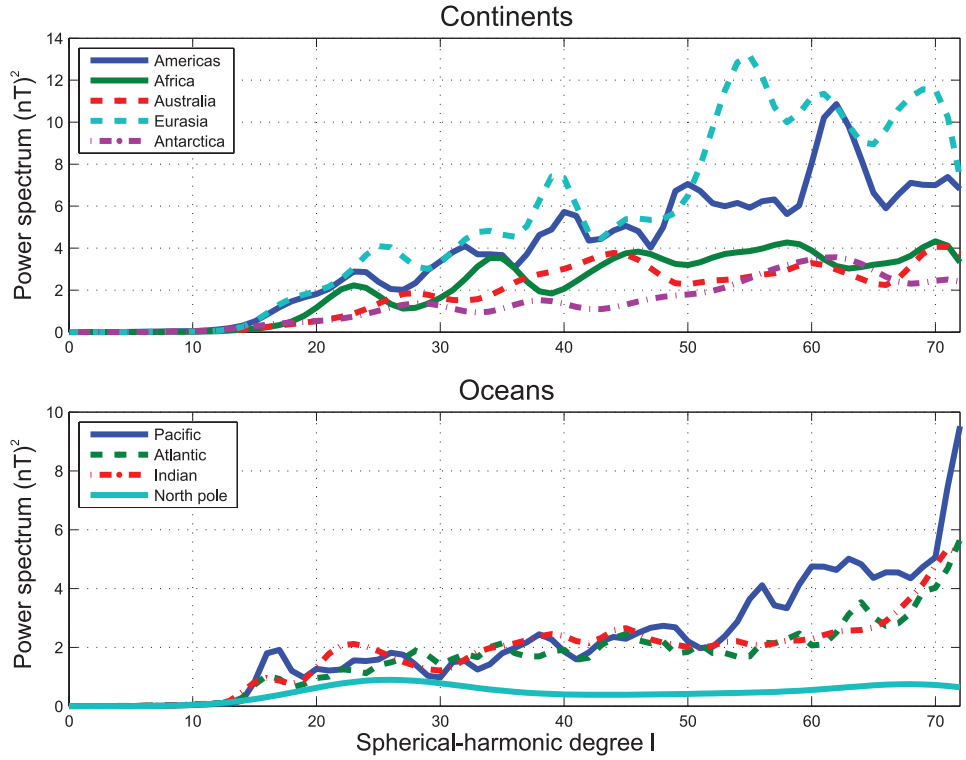

Figure 5. The power spectrum of the crustal magnetic field decomposed into nine different regions. Continental regions are presented in the upper plot and oceanic regions are in the lower one. The sum of the partial spectra is a very good approximation to the global spectrum. Units: nT^2.

Fig. 5 shows the power spectra of the decomposed regions. The sum of the partial spectra for these nine parts approximates very well, but does not exactly match, the global MF7 spectrum. There are similar contrasts between continental and oceanic signals as noted previously. For instance, continental spectra seem to 'flatten' towards the highest harmonic degrees, while the oceanic spectra tend to start to increase at higher degrees. There is much greater roughness in the spectra of the continental regions than in those of the oceanic ones. Eurasia and the Americas, in particular, show most departure from a smooth curve, exhibiting a series of crests and troughs in their spectra. The spectrum of the Americas contains one prominent peak close to degree 60 whereas that of Eurasia contains at least three peaks and displays overall much greater power within the degree range 50–70 than any other continental region. All of the continental regions are characterized by power that diminishes significantly from the higher to the lower degrees.

In the oceanic signals, only the Pacific spectrum contains a clear peak at degree 16, which was notable in the all-oceanic signal shown in Fig. 3. Hence, whatever the cause of this long-wavelength variation, it most likely originates in the Pacific Ocean. The Pacific Ocean spectrum also exhibits much more variability than that of other oceanic regions. However, it does not account for much greater power than the spectra of the Atlantic or Indian Oceans, although its area is twice as large. There are also differences in smoothness of the spectra. The Pacific and Atlantic Ocean spectra are much less smooth than those for most of the continental regions, except for

that of the Americas, which also exhibits abrupt changes in slope. The North Pole is included in the oceanic areas, but it is questionable whether it is possible to obtain any information from the area by this analysis, as the area of the region is less than 1 per cent of the whole globe and it lies within the satellite polar gap. Thus it is unlikely to have significant information or power at any of the wavelengths analysed here.

3.4 Spectral coupling in the decomposed signals

Quantifying the spectral coupling or leakage within a decomposed signal allows us to determine the resolution of our power spectral results. The coupling is related to the size of the region of interest, its shape, the degree resolution of the model and the truncation level of the bases. Coupling between degrees and orders arises from the separation of the matrix $\mathbf{G}^{\mathrm{T}}$ that we encountered in eq. (11), which breaks its unitarity. Summation over the orders in the squared $\mathbf{G}_{\mathrm{in}}\mathbf{G}_{\mathrm{in}}^{\mathrm{T}}$ and $\mathbf{G}_{\mathrm{out}}\mathbf{G}_{\mathrm{out}}^{\mathrm{T}}$ projection matrices quantifies the spectral coupling between individual degrees in the power spectral estimate of eq. (5) made with Gauss coefficients transformed via eqs (22) and (23), by analogy with properties of spectral estimators discussed by Dahlen & Simons (2008, their eqs 57, 131 and 140). For example, the spectral coupling matrix $\mathbf{C}_{\mathrm{in}} = (\mathbf{G}_{\mathrm{in}}\mathbf{G}_{\mathrm{in}}^{\mathrm{T}})^2$ for the 'in' region yields a $(73^2 \times 73^2)$ matrix. The coupling value for each degree l is computed by summing over the orders of $\mathbf{C}_{\mathrm{in}}$, and dividing by $(2l + 1)$, resulting in a (73×73) matrix. Ideally, these summation matrices should closely approximate the identity matrix, indicating a lack of coupling between degrees (but remember that eq. 5 contains a sum over the orders), but such a situation is not generally achievable when regional resolution over partial spatial domains is being sought.

Fig. 6 shows the values of the coupling matrices for low-pass degree 0–72 Slepian functions with Shannon-number truncation. The behaviour of the bandpass functions is qualitatively similar and

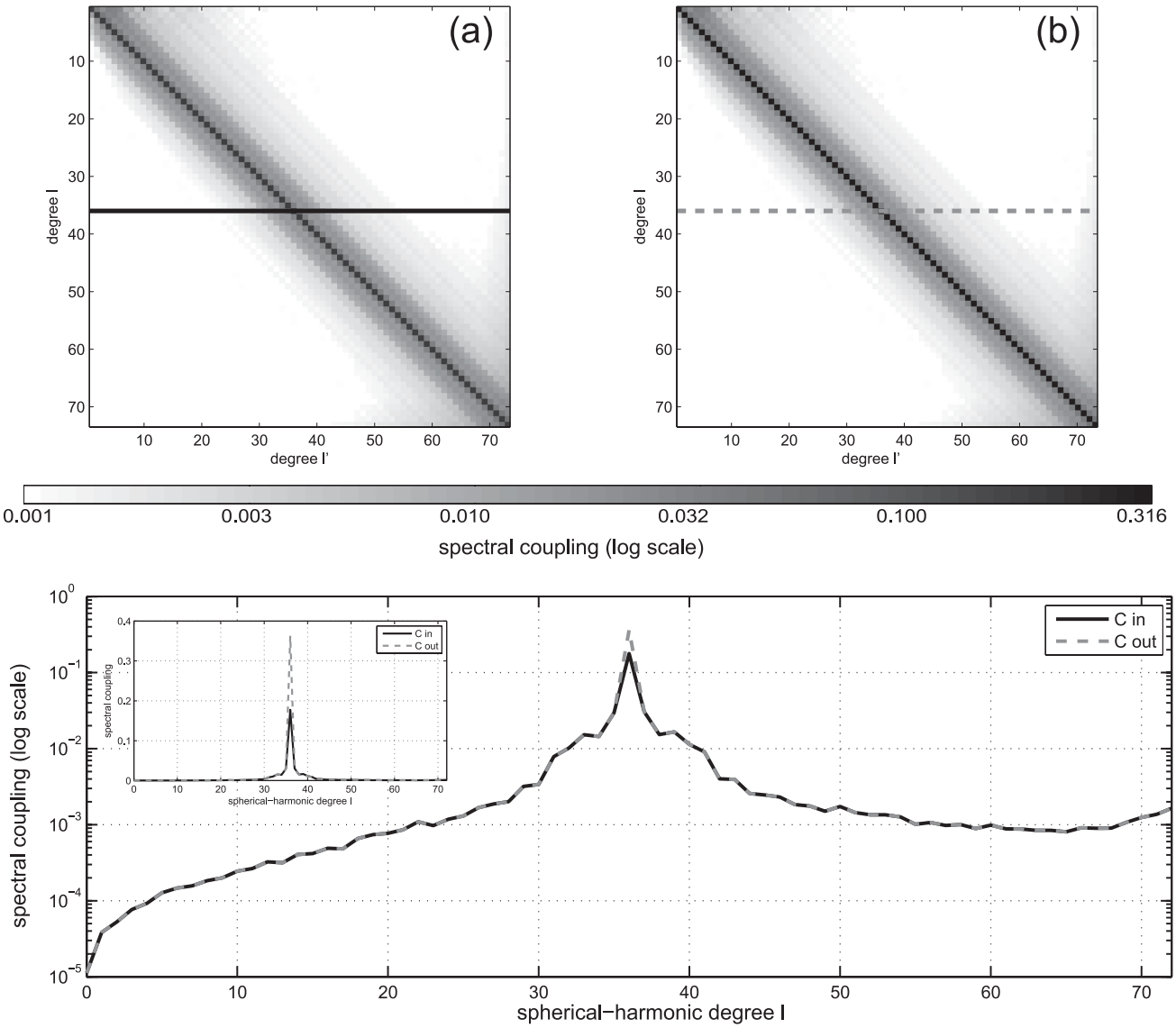

Figure 6. Coupling matrices for the spherical-harmonic power spectrum of the domain-decomposed fields. (a) Coupling when using $K = 2170$ Slepian functions to concentrate over the continents, and (b) when using $(L - 1)^2 - K = 3159$ Slepian functions over the oceans. The values shown at each degree contain the normalization factor $(2l + 1)$, as defined in Section 3.4. The lower panel shows the coupling of degree $l = 36$ of the continental (solid black) and oceanic (dashed grey) decomposition, on a log scale. A linear plot of the same data is shown in the left-hand corner.

will not be illustrated here. The coupling is plotted on a logarithmic scale to emphasize the detail in the matrices. Coupling is evident between degrees 0 and 15 which accounts for the spectral leakage seen in Fig. 3. From degrees 16–72 the coupling of both regions shows a strong peak at the central degree, with narrow flanks. The lower panel of Fig. 6 shows the coupling of degree $l = 36$ for the continental 'in' and oceanic 'out' domains (i.e. the 37th row of the low-pass coupling matrices). There is a strong peak at the target degree, with narrow shoulders falling to approximately zero at about six spherical-harmonic degrees on either side. Except at the low-degree and high-degree edges of the domain, the coupling matrices are roughly constant-diagonal, which implies that in the interior the bandwidth of our spectral estimate is about 12 spherical-harmonic degrees. The effective bandwidth, in terms of its full-width at half height, is much smaller than that, only about two or three degrees. Information from degrees outside this band does not couple strongly into the spectral estimate of the decomposed fields at the target. A comparison of this coupling with the behaviour of the 'periodogram' and '(multi)taper' estimates, derived and depicted by Dahlen & Simons (2008, their Figs 4–7), illustrates that the method employed in this paper is an effective way of localizing the power spectral estimate both in the spatial and spectral domains.

To give a visual sense of how spectral coupling works under our procedure, we illustrate it by simply decomposing models containing only one or a few individual spherical-harmonic degrees at a time. Using only coefficients from one spherical-harmonic degree (and including all orders of that degree) of the global model, we decompose it into oceanic and continental regions. The first such experiment is shown in Fig. 7(a). We then progressively add one extra model degree at a time, successively decomposing these synthesized fields into continental and oceanic parts, and calculating the power spectrum, as shown in Figs 7(b)–(d) . The four spherical-harmonic degrees are chosen from the higher end of the spectrum where continental crust dominates, specifically degrees 55, 61, 64 and 68, where prominent peaks were seen to occur in Fig. 3.

Fig. 7 shows the spectra of these decomposed signals. The peaks as recovered relate to the input power spectrum via convolution with the spectral coupling matrices of Fig. 6, as first shown by Wieczorek & Simons (2005 2007) and generalized by Dahlen & Simons (2008, their eqs 59, 135 and 140). Thus, the result for the single spike in Fig. 7(a) is similar to the curves from the cross-section of the coupling matrices in Fig. 6. As our spectral mean squares refer to the whole sphere, and not just to the area of the

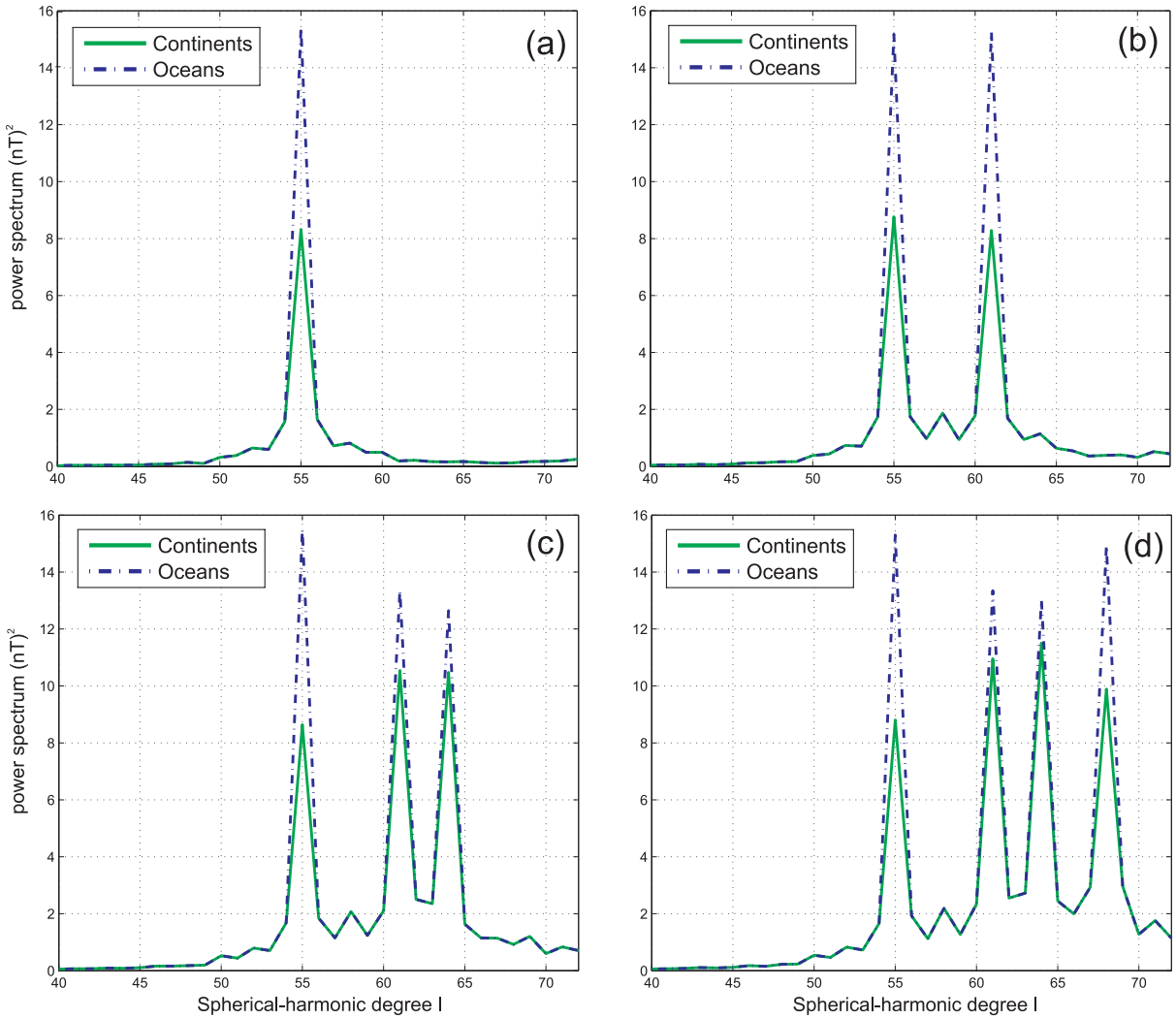

Figure 7. Decomposing strong peaks in the MF7 spectrum into oceanic and continental signals. These are taken at the four peaks in the global spectrum within degrees 55–68. First the data of (a) one peak ($l = 55$), then the data of (b) two peaks ($l = 55$ and 61), then (c) three peaks ($l = 55$, 61 and 64) and finally (d) all four peaks ($l = 55$, 61, 64 and 68) are analysed. Units: nT^2.

continents or oceans, due to its greater area, the power spectrum in the oceanic signal is greater than that of the continents. If instead of the low-pass Slepian functions, their bandpass versions are being used, all relationships between degrees are altered, but the procedure for their evaluation remains identical. The spectral coupling matrix contains the information on the blurring that is caused by the particular decomposition, and spike tests can be performed for visual guidance. The bandpass and low-pass Slepian-function model decompositions are different. Since the crustal-field model does not contain the lowermost degrees, neither should the decomposed signals. For this reason, we prefer the analysis using the bandpassed Slepian functions, although Figs 3 and 4 show that the interpretative differences will be minor.

When the power spectrum shows significant roughness, or when the spectrum has a local slope that is significantly different from zero (indicating a 'non-flat' spectral process), the coupling between spherical-harmonic degrees induced by the decomposition will lead to estimates that are significantly biased, as they would be with any other partial-domain method (Dahlen & Simons 2008). In contrast, the spectral estimates for smoothly varying, flat or 'moderately coloured' spectra will be approximately unbiased, if properly scaled. The interpretation of what constitutes 'moderate' colouring is to be made with reference to the effective bandwidth of the spectral estimator. The comparison of the global power spectra in Figs 3 and 4 with the effective bandwidth of the estimator, as apparent from Fig. 6, suggests that this interpretative approximation is justified. We thus conclude that the decomposition of the global crustal magnetic field using Slepian functions into oceanic and continental portions not only provides an excellent approximation to the individual fields in the space domain, but also leads to useful and reliable representations of their power spectra. A complete multitaper analysis in the vein of Dahlen & Simons (2008, their Section 7) would provide more control over the variance of the power spectral estimate, but given the clear-cut spectral separation of the source model after the spatial decomposition in the case of the magnetic field, the benefits would be largely statistical. However, should the spectrum need to be known with its uncertainty to map this into uncertainties on model parameters derived from it, such an approach might still be preferable, as shown by Lewis & Simons (2012) for the Martian magnetic field.

4 DISCUSSION

In this work we employed spatio-spectrally concentrated spherical Slepian functions to decompose global geomagnetic models, available as spherical-harmonic expansion coefficients, into their regional contributions. Our experiments with the terrestrial lithospheric field indicate that there is a clear difference between the magnetic signature of continents versus oceans, and provide a quantitative basis for its interpretation.

First, the continental field carries more than twice as much energy (mean-squared field over the sphere summed over all available harmonics, defined in eq. 5) as the oceanic field, although the continental area is only ∼40 per cent of the surface. This can be explained by the larger volume of the continental crust, although it should be counterbalanced to some extent by extrusive oceanic basaltic layers with strong magnetization (Purucker *et al.* 2003; Gubbins *et al.* 2011). Secondly, the oceanic signal contains approximately equal total power at all degrees, whereas the shape of the continental power spectrum resembles that of the whole field (increasing towards higher degrees and flattening slightly towards the end).

The oceanic spectrum arises from a combination of processes, some natural and some inherent in the data processing, such as randomly timed reversals of magnetic poles, non-uniform plate motions and the smoothing effect of the satellite measurements from which MF7 is derived. We conclude that the young, steadily regenerating oceanic crust contains approximately equal power over all degrees, whereas the more mature, slowly evolving, crust of the continents possesses significantly more power in the higher degrees, due to the thickness of the continents and the nature of their amalgamation.

As an additional experiment, we decomposed the historical core field of the model *gufm1* at the CMB (Jackson *et al.* 2000) into regions of anomalously slow seismic shear wave velocities and their complement (Grand 2002). These decompositions were produced for every 10 yr for the time period 1590–1990, with the results indicating that, approaching the present date, the spectral signatures of the decomposed regions become increasingly indistinct, suggesting that few unambiguously resolvable differences exist between them. However, we concluded from examination of the coupling matrices that when the range of spherical harmonics degrees is limited, such as is the case with the core field, the spatio-spectral decomposition is not sufficiently discriminant to justify strong conclusions.

5 CONCLUSIONS

Using spherical Slepian functions, both in their traditional low-pass (for the degrees 0–72) and novel bandpass (for degrees 16–72) incarnations, we decomposed the global lithospheric magnetic field model MF7, complete to spherical-harmonic degree and order 72, into two regions: one that is localized over the continents, and its complement which is localized in the ocean basins. The results demonstrate that the continental region dominates the lithospheric magnetic field, and also that the two regions have very distinct spectral signatures. The oceanic signal appears to have approximately equal power across all spherical-harmonic degrees while the continental signal shows increasing power as a function of degree.

Our method provides interpretable decompositions when the data set has a smoothly varying spectrum (with respect to the effective coupling bandwidth of the spectral estimate) and when the range of spherical-harmonic degrees is sufficiently large. The lithospheric field was a prime candidate for our analysis; in contrast, the core field does not meet these criteria.

The analysis using Slepian functions is one of a range of localization methods that are applicable to a large number of (geophysical) studies where spherical-harmonic modelling is used. The key advantages of Slepian functions are their harmonicity and double orthogonality, both over the region of interest and over the whole sphere, their ease of calculation, and their possible application as basis functions to conduct linear inverse problems, or as windowing functions to perform quadratic spectral analysis. Each of those aspects has received a thorough theoretical treatment in prior work. The method developed in this paper represents a hybrid form, whereby we approximated the signal of interest inside of the individual regions of study using a truncated Slepian expansion, and subsequently, we employed the traditional Mauersberger–Lowes spherical-harmonics-based power-spectral estimation on the space-domain results. We have shown how this resulted in appropriately spatio-spectrally concentrated estimates both of the underlying signals and their power spectra, and we showed how to interpret the resolution of the resulting spectral estimate via a characterization of its coupling (or leakage) kernel.

ACKNOWLEDGEMENTS

We sincerely thank the Editor, Richard Holme, Erwan Thébault and Frank Lowes, for their patience, their support and the detailed commentary on two earlier versions of this manuscript. This research was partly funded by the NERC GEOSPACE programme under grants NER/O/S/2003/00674 and NER/O/S/2003/00677, and is published with the permission of the Executive Director of the British Geological Survey (NERC). We acknowledge the use of the ETOPO2v2 map from the National Oceanic and Atmospheric Administration, National Geophysical Data Center, USA. FJS thanks the U.S. National Science Foundation for support under CAREER grant EAR-1150145, and Princeton University account 195-2243. Computer code to perform the analysis and generate the figures in this paper is available from http://www.frederik.net.

REFERENCES

Amirbekyan, A., Michel, V. & Simons, F.J., 2008. Parameterizing surface-wave tomopgraphic models with harmonic spherical splines, *Geophys. J. Int.,* **174**(2), 617–628.

Arkani-Hamed, J. & Dyment, J., 1996. Magnetic potential and magnetization contrasts of Earth's lithosphere, *J. geophys. Res.,* **101**(B5), 11 401–11 411.

Backus, G.E., Parker, R.L. & Constable, C.G., 1996. *Foundations of Geomagnetism,* Cambridge Univ. Press, Cambridge, UK.

Becker, T.W. & Boschi, L., 2002. A comparison of tomographic and geodynamic mantle models, *Geochem. Geophys. Geosys.,* **3**(1), doi:10.1029/2001GC000168.

Blakely, R.J., 1996. *Potential Theory in Gravity and Magnetic Applications,* Cambridge University Press.

Cohen, Y. & Achache, J., 1994. Contribution of induced and remanent magnetization to long-wavelength oceanic magnetic anomalies, *J. geophys. Res.,* **99**(B2), 2943–2954.

Counil, J.L., Cohen, Y. & Achache, J., 1991. The global continent-ocean magnetization contrast, *Earth planet. Sci. Lett.,* **103**(1–4), 354–364.

Dahlen, F.A. & Simons, F.J., 2008. Spectral estimation on a sphere in geophysics and cosmology, *Geophys. J. Int.,* **174,** 774–807.

Daubechies, I., 1992. Ten lectures on wavelets, in *Proceedings of CBMS-NSF Regional Conference Series in Applied Mathematics,* Vol. 61, Society for Industrial & Applied Mathematics, Philadelphia, PA.

Dyment, J. & Arkani-Hamed, J., 1998. Contribution of lithospheric remanent magnetization to satellite magnetic anomalies over the world's oceans, *J. geophys. Res.,* **103,** 15 423–15 441.

Freeden, W. & Michel, V., 1999. Constructive approximation and numerical methods in geodetic research today: an attempt at a categorization based on an uncertainty principle, *J. Geod.,* **73**(9), 452–465.

Friis-Christensen, E., Lühr, H. & Hulot, G., 2006. Swarm: A constellation to study the Earth's magnetic field, *Earth Planets Space,* **58,** 351–358.

Górski, K.M., 1994. On determining the spectrum of primordial inhomogeneity from the COBE DMR sky maps: method, *Astroph. J.,* **430**(2), L85–L88.

Grand, S., 2002. Mantle shear–wave tomography and the fate of subducted slabs, *Phil. Trans. R. Soc. Lond. A,* **360**(1800), 2475–2491.

Gubbins, D., Ivers, D., Masterton, S.M. & Winch, D.E., 2011. Analysis of lithospheric magnetization in vector spherical harmonics, *Geophys. J. Int.,* **187,** 99–117.

Haines, G., 1985. Spherical cap harmonic analysis, *J. geophys. Res.,* **90**(B3), 2583–2591.

Harig, C. & Simons, F.J., 2012. Mapping Greenland's mass loss in space and time, *PNAS,* **109**(49), 19 934–19 937.

Hauser, M.G. & Peebles, P.J.E., 1973. Statistical analysis of catalogs of extragalactic objects. II. The Abell catalog of rich clusters, *Astroph. J.,* **185,** 757–785.

Hipkin, R.G., 2001. The statistics of pink noise on a sphere: applications to mantle density anomalies, *Geophys. J. Int.,* **144,** 259–270.

Holschneider, M., Chambodut, A. & Mandea, M., 2003. From global to regional analysis of the magnetic field on the sphere using wavelet frames, *Phys. Earth planet. Inter.,* **135,** 107–124.

Hulot, G., Finlay, C., Constable, C., Olsen, N. & Mandea, M., 2010. The magnetic field of planet earth, *Space Sci. Rev.,* **152,** 159–222.

Hwang, C., 1993. Spectral analysis using orthonormal functions with a case study on sea surface topography, *Geophys. J. Int.,* **115,** 1148–1160.

Jackson, A., Jonkers, A. & Walker, M., 2000. Four centuries of geomagnetic secular variation from historical records, *Phil. Trans. R. Soc. London. A,* **358**(1768), 957–990 [Mathematical, Physical and Engineering Sciences].

Jolliffe, I.T., 2002. *Principal Component Analysis, 2nd edn,* Springer.

Kaula, W.M., 1967. Theory of statistical analysis of data distributed over a sphere, *Rev. Geophys.,* **5**(1), 83–107.

Kono, M., 2007. Geomagnetism in perspective, in *Treatise on Geophysics,* Vol. 5, pp. 1–31, ed. Schubert, G., Elsevier.

Langel, R.A. & Hinze, W.J., 1998. *The Magnetic Field of the Earth's Lithosphere: The Satellite Perspective,* Cambridge University Press.

Lesur, 2006. Introducing localized constraints in global geomagnetic field modelling, *Earth Planets Space,* **58,** 477–483.

Lewis, K.W. & Simons, F.J., 2012. Local spectral variability and the origin of the Martian crustal magnetic field, *Geophys. Res. Lett.,* **39,** L18201, doi:10.1029/2012GL052708.

Lowes, F.J., 1966. Mean-square values on sphere of spherical harmonic fields, *J. geophys. Res.,* **71**(8), doi:10.1029/JZ071i008p02179.

Lowes, F.J., 1974. Spatial power spectrum of the main geomagnetic field, and extrapolation to the core, *Geophys. J. R. astr. Soc.,* **36**(3), 717–730.

Mallat, S., 1998. *A Wavelet Tour of Signal Processing,* Academic Press, San Diego, CA.

Mauersberger, P., 1956. Das Mittel der Energiedichte des geomagnetischen Hauptfeldes an der Erdoberfläche und seine säkulare Änderung, *Gerlands Beitr. Geophys,* **65,** 207–215.

Maus, S., 2008. The geomagnetic power spectrum, *Geophys. J. Int.,* **174,** 135–142.

Maus, S., Lühr, H., Rother, M., Hemant, K., Balasis, G., Ritter, P. & Stolle, C., 2007. Fifth-generation lithospheric magnetic field model from CHAMP satellite measurements, *Geochem. Geophys. Geosys.,* **8**(5), doi:10.1029/2006GC001521.

Maus, S. *et al.*, 2008. Resolution of direction of oceanic magnetic lineations by the sixth-generation lithospheric magnetic field model from CHAMP satellite magnetic measurements, *Geochem. Geophys. Geosyst.,* **9**(7), doi:10.1029/2008GC001949.

Maus, S. *et al.*, 2009. EMAG2: A 2-arc min resolution Earth Magnetic Anomaly Grid compiled from satellite, airborne, and marine magnetic measurements, *Geochem. Geophys. Geosyst.,* **10**(8), doi:10.1029/2008GC001949.

Maus, S., Manoj, C., Rauberg, J., Michaelis, I. & Lühr, H., 2010. NOAA/NGDC candidate models for the 11th generation International Geomagnetic Reference Field and the concurrent release of the 6th generation Pomme magnetic model, *Earth Planet. Space,* **62,** 729–735.

Müller, R., Sdrolias, M., Gaina, C. & Roest, W., 2008. Age, spreading rates, and spreading asymmetry of the world's ocean crust, *Geochem. Geophys. Geosys.,* **9**(5), Q04006, doi:10.1029/2007GC001743.

Narcowich, F.J. & Ward, J.D., 1996. Nonstationary wavelets on the m-sphere for scattered data, *Appl. Comput. Harmon. Anal.,* **3,** 324–336.

Oh, S.P., Spergel, D.N. & Hinshaw, G., 1999. An efficient technique to determine the power spectrum from cosmic microwave background sky maps, *Astroph. J.,* **510,** 551–563.

Peebles, P. J.E., 1973. Statistical analysis of catalogs of extragalactic objects. I. Theory, *Astroph. J.,* **185,** 413–440.

Percival, D.B. & Walden, A.T., 1993. *Spectral Analysis for Physical Applications, Multitaper and Conventional Univariate Techniques,* Cambridge Univ. Press, New York.

Plattner, A. & Simons, F.J., 2013. Spatiospectral concentration of vector fields on a sphere, *Appl. Comput. Harmon. Anal.,* doi:10.1016/j.acha.2012.12.001.

Plattner, A., Simons, F.J. & Wei, L., 2012. Analysis of real vector fields on the sphere using Slepian functions, in *2012 IEEE Statistical Signal Processing Workshop (SSP'12),* Ann Arbor, USA, IEEE.

Purucker, M., Langlais, B., Olsen, N., Hulot, G. & Mandea, M., 2002. The southern edge of cratonic North America: evidence from new satellite magnetometer observations, *Geophys. Res. Lett.,* **29**(15), 8000–8003.

Purucker, M., Sabaka, T., Olsen, N. & Maus, S., 2003. How have Ørsted, CHAMP, and SAC-C improved our knowledge of the oceanic regions? In *Proceedings of the 4th OIST Conference,* Copenhagen, Denmark.

Reigber, C., Schmidt, R., Flechtner, F., König, R., Meyer, U., Neumayer, K.-H., Schwintzer, P. & Zhu, S., 2005. An Earth gravity field model complete to degree and order 150 from GRACE: EIGEN-GRACE02S, *J. Geodyn.,* **39,** 1–10.

Ritsema, J.A., Deuss, A., van Heijst, H.J. & Woodhouse, J.H., 2010. S40RTS: a degree-40 shear-velocity model for the mantle from new Rayleigh wave dispersion, teleseismic traveltime and normal-mode splitting function measurements, *Geophys. J. Int.,* **184,** 1223–1236.

Sabaka, T.J., Hulot, G. & Olsen, N., 2010. Mathematical properties relevant to geomagnetic field modeling, in *Handbook of Geomathematics,* Chapter 17, pp. 503–538, eds Freeden, W., Nashed, M.Z. & Sonar, T., Springer, Heidelberg, Germany.

Schachtschneider, R., Holschneider, M. & Mandea, M., 2010. Error distribution in regional inversion of potential field data, *Geophys. J. Int.,* **181,** 1428–1440.

Schachtschneider, R., Holschneider, M. & Mandea, M., 2012. Error distribution in regional modelling of the geomagnetic field, *Geophys. J. Int.,* **191,** 1015–1024.

Schott, J.J. & Thébault, E., 2011. Modelling the Earth's magnetic field from global to regional scales, in *Geomagnetic Observations and Models, Vol. 5 of IAGA Special Sopron Book Series,* pp. 229–264, eds Mandea, M. & Korte, M., Springer.

Shure, L., Parker, R.L. & Backus, G.E., 1982. Harmonic splines for geomagnetic modelling, *Phys. Earth planet. Inter.,* **28,** 215–229.

Shure, L., Parker, R.L. & Langel, R.A., 1985. A preliminary harmonic spline model from Magsat data, *J. geophys. Res.,* **90,** 11505–11512.

Simons, F.J., 2010. Slepian functions and their use in signal estimation and spectral analysis, in *Handbook of Geomathematics,* Chapter 30, eds Freeden, W., Nashed, M. Z. & Sonar, T., Springer.

Simons, F.J. & Dahlen, F.A., 2006. Spherical Slepian functions and the polar gap in geodesy, *Geophys. J. Int.,* **166,** 1039–1061.

Simons, F.J., Dahlen, F.A. & Wieczorek, M.A., 2006. Spatiospectral concentration on a sphere, *SIAM Rev.,* **48**(3), 504–536.

Simons, F.J., Hawthorne, J.C. & Beggan, C.D., 2009. Efficient analysis and representation of geophysical processes using localized spherical basis functions, in *Wavelets XIII,* Vol. 7446, pp. 74460G, SPIE.

Simons, M., Solomon, S.C. & Hager, B.H., 1997. Localization of gravity and topography: constraints on the tectonics and mantle dynamics of Venus, *Geophys. J. Int.,* **131,** 24–44.

Slepian, D., 1983. Some comments on Fourier analysis, uncertainty and modeling, *SIAM Rev.,* **25**(3), 379–393.

Slobbe, D.C., Simons, F.J. & Klees, R., 2012. The spherical Slepian basis as a means to obtain spectral consistency between mean sea level and the geoid, *J. Geod.,* **86**(8), 609–628.

Spencer, C. & Gubbins, D., 1980. Travel-time inversion for simultaneous earthquake location and velocity structure determination in laterally varying media, *Geophys. J. R. astr. Soc.,* **63**(1), 95–116.

Tegmark, M., 1996. A method for extracting maximum resolution power spectra from microwave sky maps, *Mon. N. R. astr. Soc,* **280,** 299–308.

Tegmark, M., 1997. How to measure CMB power spectra without losing information, *Phys. Rev. D,* **55**(10), 5895–5907.

Thébault, E., Schott, J.J. & Mandea, M., 2006. Revised spherical cap harmonic analysis (RSCHA): validation and properties, *J. geophys. Res.,* **111,** doi:10.1029/2005JB003836.

Thébault, E., Hemant, K., Hulot, G. & Olsen, N., 2009. On the geographical distribution of induced time-varying crustal magnetic fields, *Geophys. Res. Lett.,* **36,** doi:10.1029/2008GL036416.

Thébault, E., Purucker, M., Whaler, K.A., Langlais, B. & Sabaka, T.J., 2010. The magnetic field of the Earth's lithosphere, *Space Sci. Rev.,* **155,** 1–33.

Thomson, A.W.P., Hamilton, B., Macmillan, S. & Reay, S.J., 2010. A novel weighting method for satellite magnetic data and a new global magnetic field model, *Geophys. J. Int.,* **181**(1), 250–260.

Trampert, J. & Snieder, R., 1996. Model estimations biased by truncated expansions: possible artifacts in seismic tomography, *Science,* **271**(5253), 1257–1260.

Wandelt, B.D., Hivon, E. & Górski, K.M., 2001. Cosmic microwave background anisotropy power spectrum statistics for high precision cosmology, *Phys. Rev. D,* **64**(8), 1–14.

Whaler, K.A. & Gubbins, D., 1981. Spherical harmonic analysis of the geomagnetic field: an example of a linear inverse problem, *Geophys. J. Int.,* **65**(3), 645–693.

Wieczorek, M.A. & Simons, F.J., 2005. Localized spectral analysis on the sphere, *Geophys. J. Int.,* **162**(3), 655–675.

Wieczorek, M.A. & Simons, F.J., 2007. Minimum-variance spectral analysis on the sphere, *J. Fourier Anal. Appl.,* **13**(6), 665–692.

Xu, P., 1998. Truncated SVD methods for discrete linear ill-posed problems, *Geophys. J. Int.,* **135**(2), 505–514.